

# NASimJax: GPU-Accelerated Policy Learning Framework for Penetration Testing

Raphael Simon<sup>1,2\*</sup>      José Carrasquel<sup>1</sup>      Wim Mees<sup>1</sup>  
 Pieter Libin<sup>2</sup>

<sup>1</sup>CISS Department, Royal Military Academy, Belgium  
<sup>2</sup>AI Lab, Vrije Universiteit Brussel, Belgium

## Abstract

Penetration testing—the practice of simulating cyberattacks to identify vulnerabilities—is a complex sequential decision-making task that is inherently partially observable and features large action spaces. Training reinforcement learning (RL) policies for this domain faces a fundamental bottleneck: existing simulators are too slow to train on realistic network scenarios at scale, resulting in policies that fail to generalize. We present NASimJax, a complete JAX-based reimplementation of the Network Attack Simulator (NASim), achieving up to 100× higher environment throughput than the original simulator. By running the entire training pipeline on hardware accelerators, NASimJax enables experimentation on larger networks under fixed compute budgets that were previously infeasible. We formulate automated penetration testing as a Contextual POMDP and introduce a network generation pipeline that produces structurally diverse and guaranteed-solvable scenarios. Together, these provide a principled basis for studying zero-shot policy generalization. We use the framework to investigate action-space scaling and generalization across networks of up to 40 hosts. We find that Prioritized Level Replay better handles dense training distributions than Domain Randomization, particularly at larger scales, and that training on sparser topologies yields an implicit curriculum that improves out-of-distribution generalization, even on topologies denser than those seen during training. To handle linearly growing action spaces, we propose a two-stage action decomposition (2SAS) that substantially outperforms flat action masking at scale. Finally, we identify a failure mode arising from the interaction between Prioritized Level Replay’s episode-reset behaviour and 2SAS’s credit assignment structure. NASimJax thus provides a fast, flexible, and realistic platform for advancing RL-based penetration testing.

## 1 Introduction

Cybersecurity has become one of the most critical domains in modern society, underpinning healthcare, banking, and energy infrastructure. Among the tools used to proactively defend these systems is penetration testing — the authorised practice of simulating attacks to identify vulnerabilities and misconfigurations in IT networks [National Institute of Standards and Technology, 2008]. While effective, penetration testing is laborious and expensive, requiring seasoned security experts to reason over long decision horizons, weigh competing attack vectors, and adapt to the specifics of each target network. Automating this process via reinforcement learning (RL) has only recently gained traction [Liu et al., 2025], motivated by the success of RL in other complex sequential decision-making domains such as games [Mnih et al., 2015, OpenAI et al., 2019a, Vinyals et al., 2019, Wurman et al., 2022] robotics [OpenAI et al., 2019b], disease modelling [Cimpean et al., 2023] and industrial control [Verstraeten et al., 2020]. The penetration testing problem maps naturally onto a Partially Observable Markov Decision Process (POMDP) [Sarraute et al., 2012, 2013]: an agent cannot directly observe the full network topology or its vulnerabilities, and must actively acquire information before acting. Beyond this inherent partial observability, training effective RL policies for penetration testing faces

---

\*Corresponding author: [r.simon@cyllab.be](mailto:r.simon@cyllab.be)

challenges common to real-world RL applications [Dulac-Arnold et al., 2021] — most notably the sim-to-real gap and generalization to unseen scenarios [Liu et al., 2025]. Real-world penetration testing involves long decision horizons, sparse and delayed rewards, combinatorial action spaces, and strong dependence on network-specific structure. Policies that overfit to narrow training scenarios will fail to generalize, and closing this gap requires simulators that expose agents to structural diversity and decision-relevant complexity rather than merely increasing surface-level realism. Existing penetration testing simulators [Schwartz and Kurniawatti, 2019, Team., 2021, Emerson et al., 2024] fall short on two fronts. First, they are primarily fixed to single or narrowly parameterized scenarios, providing insufficient diversity to train generalizable policies. Second, they rely on CPU-bound Python implementations, which creates a fundamental throughput bottleneck: RL requires millions of environment interactions due to sample inefficiency, yet these simulators cannot generate experience fast enough to fully utilize modern accelerators. This bottleneck is especially costly in penetration testing, where RL algorithms are not yet well understood and thorough hyperparameter searches — crucial for reliable results in any new domain, given the known sensitivity of RL to hyperparameter choices [Patterson et al., 2024, Adkins et al., 2024] — are simply intractable at the speeds current tools offer. To address these challenges, we present NASimJax, a full JAX-based reimplement and extension of the Python-native Network Attack Simulator (NASim) [Schwartz and Kurniawatti, 2019]. NASimJax preserves the core task abstraction of NASim — modelling penetration testing as a partially observable sequential decision process — but substantially reworks the environment design to support distributional training, curriculum learning, and context-dependent generalization. By running the entire training pipeline on hardware accelerators, NASimJax enables vectorized training across thousands of parallel environment instances, eliminating the CPU-GPU communication bottleneck and achieving up to  $100\times$  speed-up over the original (cf. Figure 2). This throughput unlocks experimentation on larger and more complex networks under fixed compute budgets, and makes broader hyperparameter search tractable under realistic compute constraints.

Beyond computational improvements, NASimJax introduces several conceptual advances. We formulate automated penetration testing as a Contextual POMDP [Ghosh et al., 2021], where each episode is conditioned on a context describing the underlying network instance. This provides a principled framework for training policies across a distribution of environments and directly facilitates zero-shot policy generalization [Kirk et al., 2023] to previously unseen networks. Realizing this formulation required a fundamental redesign of the network generation process: NASimJax introduces a new generation function that produces structurally diverse, realistic, and guaranteed-solvable scenarios, enabling fine-grained control over topology and vulnerability density. To address the linearly growing action space of larger networks, we introduce a two-stage action selection (2SAS) mechanism that decomposes each decision into host selection followed by per-host action selection. Building on this setup, we evaluate Domain Randomization (DR) [Tobin et al., 2017] and PLR [Jiang et al., 2021a] for zero-shot policy transfer, finding that low-density training yields an implicit curriculum that improves out-of-distribution generalization. This even holds on topologies denser than those seen during training. We further identify a failure mode arising from the interaction between PLR’s episode-reset behaviour and 2SAS’s credit assignment structure.

## 2 Preliminaries

### 2.1 Contextual Reinforcement Learning Setting

We formalize our setting as a contextual reinforcement learning problem. We begin with the standard MDP definition and progressively extend it to partially observable and contextual settings.

**Markov Decision Process** An MDP [Puterman, 1990] is a tuple  $\langle \mathcal{S}, \mathcal{A}, \mathcal{P}, \mathcal{R}, \rho_0, \gamma \rangle$  where  $\mathcal{S}$  is the state space,  $\mathcal{A}$  is the action space,  $\mathcal{P}(s'|s, a)$ , is the transition probability distribution over next states, conditioned on the current state and action;  $\mathcal{R} : \mathcal{S} \times \mathcal{A} \times \mathcal{S} \rightarrow \mathbb{R}$ , a reward function;  $\rho_0 \in \Delta(\mathcal{S})$ , the initial state distribution, from which an initial state can be sampled:  $s_0 \sim \rho_0$ ; and  $\gamma \in [0, 1]$  a discount factor, that determines the relative weighting of future rewards. The objective is to learn a policy  $\pi(a|s)$ , a probability distribution over actions conditioned on the current state, that maximizes the expected cumulative discounted reward  $\mathbb{E}_\pi[G_0]$  where  $G_t = \sum_{k=0}^{\infty} \gamma^k r_{t+k}$  is called the return.  $r_t$  is a random variable that represents the

reward obtained at time step  $t$ . In finite-horizon tasks the sum is clipped to  $T$ , the maximum number of allowed steps.

**Partially Observable Markov Decision Process** A POMDP [Sutton and Barto, 2018] extends the MDP framework to a tuple  $\langle \mathcal{S}, \mathcal{A}, \mathcal{P}, \mathcal{R}, \Omega, \mathcal{O}, \rho_0, \gamma \rangle$ , where  $\Omega$  represents the observation space and  $\mathcal{O}(o|s', a)$  defines the observation function. The agent does not directly observe the underlying state. Only parts of it can be observed at a given time through  $\mathcal{O}$ . The optimal policy now depends on the history of observations or belief state  $b_t \in \Delta(\mathcal{S})$ .

**Contextual Markov Decision Process** Following [Hallak et al., 2015] and the formulation adopted in [Kirk et al., 2023], a Contextual Markov Decision Process (CMDP) is a special class of POMDP with a context variable  $c \in \mathcal{C}$ , where  $\mathcal{C}$  denotes the context space and  $c$  is sampled at the beginning of each episode from a distribution  $p(c)$ . Conditioned on  $c$ , the environment induces a POMDP with context-dependent dynamics and rewards. Formally, a contextual POMDP is defined by the tuple  $\langle \mathcal{S}, \mathcal{A}, \mathcal{P}_c, \mathcal{R}_c, \Omega, \mathcal{O}_c, \rho_{0,c}, \gamma, \mathcal{C}, p(c) \rangle$ , where  $\mathcal{P}_c(s' | s, a)$  and  $\mathcal{R}_c(s, a)$  denote the transition and reward functions parameterized by  $c$ ,  $\mathcal{O}_c(o | s', a)$  is the observation function, and  $\rho_{0,c}$  is the initial state distribution conditioned on  $c$ . The joint distribution over context and initial state factorizes as  $p(c, s_0) = p(c) \rho_{0,c}(s_0)$ . The context remains fixed throughout an episode but varies across episodes according to  $p(c)$ , thereby inducing a distribution over tasks. The objective is to learn a policy that maximizes expected return under the context distribution, i.e.,  $\mathbb{E}_{c \sim p(c)} [\mathbb{E}_\pi [G_0 | c]]$ .

## 3 Related Work

### 3.1 JAX and Hardware-Accelerated RL

JAX [Bradbury et al., 2018] is a Python library for accelerator-oriented array computation and program transformation, designed for high-performance numerical computing and large-scale machine learning. Its core features — just-in-time (JIT) compilation and functional transformations such as `vmap` — make it particularly well suited for RL workloads, where tight coupling between environment simulation and policy optimization is critical. By requiring adherence to functional programming principles, JAX enables the entire training loop, including both environment stepping and policy updates, to be compiled and executed on accelerators. This eliminates the CPU-GPU communication overhead that plagues conventional Python-based RL frameworks [Rutherford et al., 2024], where the environment typically runs on the CPU while the policy trains on the GPU. Beyond compilation gains, `vmap` enables vectorization of the environment’s `step` and `reset` functions, allowing large batches of experience to be collected and processed in parallel. The adoption of JAX-based RL environments has only recently begun, with examples including the Gymnax suite [Lange, 2022], Craftax [Matthews et al., 2024], Jumanji [Bonnet et al., 2024].

### 3.2 Penetration Testing Simulators

There exist several different penetration testing environments targeted at learning RL policies. NASim [Schwartz and Kurniawatti, 2019] has been one of the first and therefore featured in several subsequent works. NASimEmu [Janisch et al., 2023] and PenGym [Nguyen et al., 2025], are extensions to NASim that bring forward an emulation component, allowing to learn policies in small simulated networks and transfer them to an emulated network consisting of virtual machines. StochNASim [Simon et al., 2025] features stochastic environment resets and networks of varying sizes to learn robust penetration testing policies. `CyberBattleSim` [Team., 2021] aims at simulating the phase of lateral movement (moving between hosts) in a network. `CybORG++` [Emerson et al., 2024] simulates both offensive and defensive agents and their dynamics within the same network. `C-CyberBattleSim` [Terranova et al., 2025], concentrates on the generation of more realistic scenarios through real-world information sources, such as vulnerability databases and security scanners—elements that are added to the network nodes as additional information.

## 4 NASimJax

We now describe the RL environment provided by NASimJax. We first outline the underlying task and abstraction, before detailing the state and observation spaces, action space, and reward function, and then describing how learning contexts are defined.

The environment is designed as a research abstraction rather than a fixed benchmark scenario. Its primary goal is to support controlled variation over network instances, enabling research on policy robustness and generalization beyond fixed scenarios. Through a versatile and stochastic network generation process, the environment can be scaled in complexity and difficulty, allowing it to remain challenging as RL algorithms improve and preventing overfitting to narrowly defined scenarios.

NASimJax models automated penetration testing as a sequential decision-making problem under partial observability. An agent interacts with a network by performing actions such as scanning hosts, enumerating services, exploiting vulnerable software to obtain an initial foothold, and escalating privileges through vulnerable processes. Information about the network topology, running services, and vulnerabilities must be actively acquired through interaction. Progress through the network is inherently sequential and long-horizon, as successful exploitation of certain hosts may be required to reach others. An episode terminates once the agent has obtained the required privileges on a predefined set of sensitive hosts.

Each episode is conditioned on a learning context, which we also call scenario, represented by a concrete network instance. A context consists of a set of hosts partitioned into subnets, connectivity rules defining how subnets may communicate, and host-specific configurations such as running services, processes, and associated exploitability. While the agent’s policy is shared across episodes, the underlying context varies, providing a principled mechanism to expose the agent to diverse network structures during training. This formulation naturally supports viewing the environment as a CMDP, where generalization is achieved by learning policies that perform well across a distribution of network contexts rather than memorizing individual attack paths.

The environment adheres to the Gymnax API [Lange, 2022]. This design choice enables seamless integration with a wide range of JAX-based RL algorithms, facilitating large-scale experimentation, reproducibility, and direct comparison of learning methods within a standardized environment.

### 4.1 State Space

The state of a network is defined by two main elements: Traffic rules, describing which subnets can talk to one another, and the collective properties of all hosts. Since IT networks naturally follow a graph-structure, we represent this via an adjacency matrix. We add another dimension to the adjacency matrix to accommodate firewall rules, that determine which services are allowed to pass between subnets. The networks’ host contain the following properties: `subnet address`, `reachable`, `discovered`, `access level`, `OS`, `services`, `processes`.

The `services` and `processes` attributes encode only those services and processes that are vulnerable and therefore exploitable by the agent. They do not represent the complete set of software running on a host, but rather a filtered abstraction capturing actionable attack surfaces. As a result, hosts may have zero vulnerable services or processes, modelling systems that are correctly configured or hardened.

To make use of JAX’s parallel computation capabilities to its fullest, the host properties are batched together into one data structure. We depict this in Figure 1b. All the host properties are either one-hot encoded or represented via boolean flags. This has two advantages. First, for most operations in the state transition logic we can solely rely on boolean operations, which have a very small computational overhead. Second, state properties can be stored using unsigned integers that only use one byte in memory, reducing the overall memory footprint of the environment, therefore allowing for more parallel environments during training.

When an agent interacts with the environment, only three host values can change: *reachable*, *discovered*, and *access level*. All other values remain static after the scenario is generated. While the full state is used internally for transition dynamics, it is intentionally not exposed to the agent, reinforcing partial observability and preventing shortcut learning.

## 4.2 Action Space

The action space is discrete and consists of six action types, grouped into reconnaissance and exploitation actions. The four reconnaissance actions are **OS Scan**, **Process Scan**, **Service Scan**, and **Subnet Scan**. The first three retrieve host-specific information, while the subnet scan enables the discovery of additional hosts and subnets once sufficient privileges have been obtained on a target host. The two exploitation actions are **Exploit** and **Privilege Escalation**. Exploits are remote actions targeting vulnerable services to gain initial access to a host, whereas privilege escalation actions leverage vulnerable processes to elevate access privileges after a foothold has been established.

The concrete action set is generated based on the set of possible operating systems and vulnerable services and processes defined for the environment. Exploitation actions are constructed from all combinations of operating systems and services, while privilege escalation actions are constructed from all operating system and process combinations. Actions are instantiated per target host, ensuring that a sufficiently expressive set of actions exists to solve any generated network. Consequently, the size of the action space is given by  $|\mathcal{A}| = |\mathcal{H}| \times (|\mathcal{A}_{\text{scan}}| + |\mathcal{OS}| \times (|V_{\text{svc}}| + |V_{\text{proc}}|))$  where  $\mathcal{H}$  denotes the set of hosts,  $\mathcal{A}_{\text{scan}}$  the set of scan actions,  $\mathcal{OS}$  the set of possible operating systems, and  $V_{\text{svc}}$  and  $V_{\text{proc}}$  the set of vulnerable services and processes. As network complexity increases, this construction leads to a rapidly growing action space, significantly increasing exploration difficulty.

## 4.3 Observation Space

The observations perceived by the agent contain only the outcome of the executed action. The outcome depends on the action type and on whether execution was successful. Successful **OS Scans**, **Service Scans**, and **Process Scans** retrieve the corresponding properties, in addition to the host and subnet address, whereas a successful **Subnet Scan** reveals all hosts within a subnet and any connected subnets. Further, **Exploit** and **Privilege Escalation** reveal a host’s OS and service/process, and whether it is sensitive or not. Additionally, the following information is appended to the flattened observation: the encoding of the action type that was executed, and four mutually exclusive flags regarding the outcome of that action (successful, connection error, permission error, and undefined error).

## 4.4 Reward Function

Each action incurs a cost, and the reward  $r_t$  at timestep  $t$  is defined as  $-\text{cost}(a_t)$  plus any additional bonus earned. For a successful subnet scan, a discovery bonus  $V_d$  is added for each newly discovered host  $n_{dh}$  (hosts may only be discovered once), yielding  $r_t = -\text{cost}(a_t) + (V_d \times n_{dh})$ . For a successful privilege escalation, a host value bonus  $V_h$  is added, giving  $r_t = -\text{cost}(a_t) + V_h$ . In all other cases, the reward is simply  $r_t = -\text{cost}(a_t)$ .

## 4.5 Network Generation

Network generation proceeds in several stages and is designed to balance realism, diversity, and guaranteed solvability of the resulting scenarios. Each generated network represents a distinct learning context while adhering to structural constraints that ensure meaningful penetration testing tasks. Figure 1a provides an illustration for this process.

We begin by randomly distributing a fixed number of hosts  $N_h$  across a fixed number of subnets  $N_s$ . Among these subnets, two are assigned special semantic roles that remain fixed across all generated scenarios. One subnet represents the Internet and contains a single host corresponding to the attacker’s machine. A second subnet represents a demilitarized zone (DMZ), which serves as a buffer between external and internal infrastructure. All remaining subnets are treated as arbitrary internal subnets.

Host-level properties are then assigned. Each host is randomly assigned an operating system according to a fixed distribution. Services and processes are distributed independently across hosts using the service density  $svc_d$  and process density  $proc_d$  parameters, respectively. These parameters control the average number of exploitable services and processes present in the network.

Host sensitivity is assigned independently with probability  $s_d$ , i.e.,  $\text{Pr}(\text{host is sensitive}) = s_d$ . This mechanism allows the generator to model varying levels of organizational security maturity, including misconfigurations or users not following security best practices.

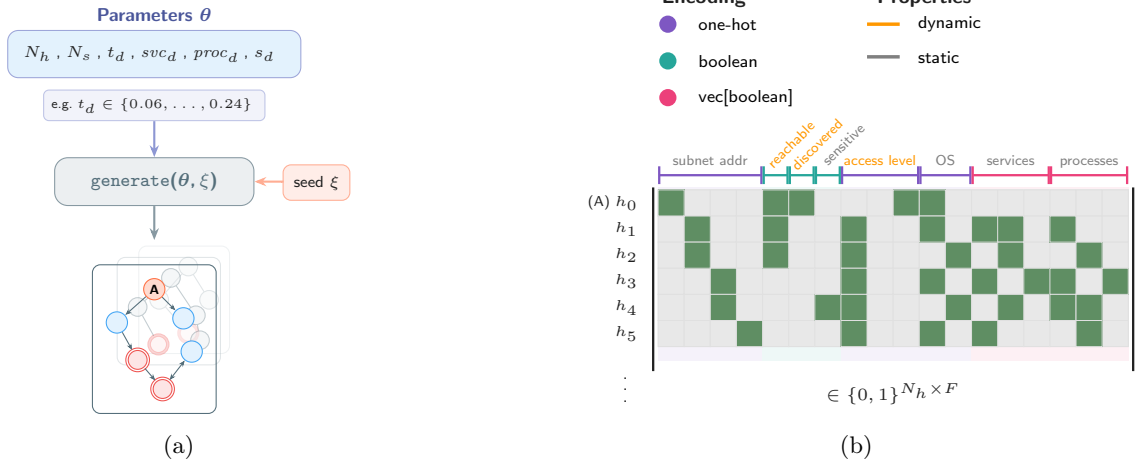


Figure 1: **Left:** Number of hosts ( $N_h$ ), and subnets ( $N_s$ ), topology ( $t_d$ ), service ( $svc_d$ ), process ( $proc_d$ ) and sensitive host density ( $s_d$ ) are all parameters that influence the generated networks. The blue nodes represent normal hosts, the red node labelled A represents the attacker’s position, and the double circled red nodes represent sensitive hosts. **Right:** Illustration of the batched state representation.  $F$  is the dimension of the host features.

To ensure that every generated scenario is solvable and supports meaningful agent interaction, we enforce several feasibility constraints after the initial random assignment. First, every subnet is guaranteed to contain at least one host running at least one service, ensuring that the agent can pivot into every subnet that becomes reachable. Second, every sensitive host is guaranteed to run at least one service and at least one process, which ensures that privilege escalation is possible on all sensitive machines. If any of these conditions are violated, the minimal number of required services or processes is added randomly to the affected hosts. These post-generation checks guarantee that successful episodes are achievable without constraining the overall diversity of generated networks.

After host and subnet properties are fixed, we generate the network topology. Connectivity between subnets is represented by an adjacency matrix of size  $N_s \times N_s$ , where entries are sampled according to the topology density parameter  $t_d$ , which controls the probability that two subnets are connected. To reflect basic network security restrictions, we impose that the Internet subnet may only communicate with the DMZ. To ensure that hosts within the same subnet can always communicate, the diagonal of the adjacency matrix is populated with ones.

The resulting topology matrix is intentionally not required to be symmetric, meaning that connections between subnets are directed. Combined with the random sampling process, this asymmetry can lead to subnets that are unreachable from the attacker’s starting position. Such subnets effectively become inactive for a given episode. While this may reduce the number of reachable hosts, it serves an important role in shaping the learning problem. Networks with fewer reachable subnets induce shorter horizons and smaller effective state spaces, whereas fully connected networks result in more complex attack paths. This mechanism provides a natural way to generate a curriculum of environments with varying difficulty levels without explicitly staging scenarios.

Although the total number of hosts  $N_h$  is fixed in order to allocate static memory layouts required for JIT compilation, the number of active hosts—those belonging to reachable subnets—varies across generated networks. As a result, a distribution over effective problem sizes is obtained even when  $N_h$  is held constant. This property enables curriculum learning by exposing agents to scenarios of increasing complexity during training. We illustrate this variability empirically in Section 6.2.

In addition to fully random host configurations, we support the generation of homogeneous subnets to better reflect real-world network administration practices, where hosts within the same subnet are often configured with similar software stacks. In this mode, services and processes are sampled jointly for all hosts in a subnet from Beta distributions parameterized by  $svc_d$  and  $proc_d$ . This approach allows controlled

variation in intra-subnet diversity while preserving the overall density of services and processes.

## 4.6 Context Sets

The design of the environment allows for several context sources. One approach is to simply use a seed, which then influences the random number generators used during the network generation phase. Train and evaluation phases can as such be seeded differently [Cobbe et al., 2019]. Further, generation parameters may be changed, to create denser or more sparse networks. The process and service density in hosts, describing how many of them are vulnerable, can also be adjusted. Changing these parameters provides the opportunity to evaluate on out-of-distribution networks, and assess zero-shot transfer capabilities of policies as discussed in [Kirk et al., 2023]. Importantly, the context  $c$  is not included in the agent’s observations; the agent must act under uncertainty about the current network configuration, inferring relevant information through interaction. This corresponds to the unobserved-context case of the CMDP as described by Kirk et al. [2023].

# 5 Methodology

## 5.1 Algorithms

We now present the selected algorithms and methods. Our implementation is based on the pure JAX PPO implementation from Lu et al. [2022]. PPO has been widely used and shown successes in most areas of RL. This field is no exception, and many other works have used it to learn policies for penetration testing [Li et al., 2023, Terranova et al., 2024, Simon et al., 2025]. As the environment is both partially observable and features a growing action space as the number of hosts increases, we discuss the choices that have been made to help learn with these challenges.

### 5.1.1 Partial Observability

To handle the challenge of partial observability, we follow the methodology described by Simon et al. [2025], where the most recent observation is kept and the accumulated history of past observations is appended. It has been shown to be effective in such sequential information retrieval environments. This approach is analogous to how human penetration testers operate, by keeping track of scan results to decide which actions to take next on the target hosts.

### 5.1.2 Large Action Spaces

To learn in large action spaces, we test two distinct methods: action masking, and a more sophisticated approach whereby we condition the action to be executed on the selected host.

**Action Masking** In RL, a substantial portion of the training budget can be wasted on actions that are invalid in the current state. Action masking has been widely used in the literature to address this issue [OpenAI et al., 2019a, Vinyals et al., 2019, Kanervisto et al., 2020]. For a discrete action space, action masking modifies the categorical distribution by giving invalid actions an infinitesimal value before applying the softmax function. This results in actions whose sampling probability becomes virtually zero. Huang and Ontañón [2022] have further analysed this method, and shown that it produces valid policy gradients. In our setting, we mask all actions for hosts that have both not been discovered yet, and are not reachable. Additionally, we mask all exploits and privilege escalation actions that are invalid due to the host not running the right combination of OS and service or OS and process respectively. We chose to not mask actions that are invalid due to missing privilege levels, as this is a learnable feature contained within the environment the observations (cf. Section 4.3).

**Two-Stage Action Selection (2SAS)** In network attack simulations the flat action space grows linearly with the number of hosts, which dilutes exploration and slows learning. Inspired by the factored action decomposition used in DeepNash for Stratego—where the agent first selects a piece and then a legal move for that piece [Perolat et al., 2022]—we decompose each decision into two stages: *host selection* followed

by *action selection* on the chosen host. Concretely, the actor-critic network shares a common feature trunk and branches into two policy heads. The first head outputs a distribution over hosts, masked to exclude unreachable or undiscovered targets. Given the sampled host, a learned host embedding is concatenated with the trunk representation and passed to the second head, which outputs a distribution over per-host actions, again masked to remove invalid choices. Because each head operates over at most  $\max(H, A/H)$  categories rather than the full product  $|\mathcal{A}| = H \cdot (A/H)$ , the effective decision complexity at each stage is substantially reduced. During training we compute separate importance-sampling ratios and clipped surrogate objectives for each stage, summing the two policy losses, with independent entropy bonuses for each head. We refer to this scheme as *two-stage action selection (2SAS)*.

### 5.1.3 Reward Scaling

Since networks are procedurally generated, the number of sensitive hosts (affected by  $s_d$ ) varies across learning contexts. This leads to high variance in the cumulative reward per episode, which can destabilize value function estimation and advantage calculation. This is a known challenge when learning across tasks with differing reward magnitudes [Van Hasselt et al., 2016], and reward normalization across procedurally generated levels has been shown to be important for stable training [Cobbe et al., 2020]. To mitigate this, we scale the rewards such that the maximum potential return is approximately invariant to the network size. Specifically, for a given context  $\mathcal{C}$ , the reward  $r_t$  at each step is scaled by the theoretical maximum reward obtainable:  $\hat{r}_t = \frac{r_t}{N_s \cdot V_h}$  where  $V_h$  is the reward value for compromising a sensitive host. This ensures that the learning signal reflects the structural difficulty of a network, such as the sparsity of vulnerabilities and the number of sensitive hosts, rather than its size alone. This provides a more stable and semantically meaningful signal across the diverse distribution of network topologies.

### 5.1.4 Unsupervised Environment Design Methods

Prioritized Level Replay (PLR) [Jiang et al., 2021a] works in conjunction with procedurally generated environments, and aims to form a natural curriculum of levels that are still deemed *interesting* for the learning progression. These can be levels where the agent currently exhibits the highest regret with respect to its current policy. PLR performs gradient updates on the random levels, whereas robust PLR (denoted as PLR<sup>+</sup>) only updates the agent on the levels sampled from the buffer. This is theoretically justified and (in some domains) empirically results in higher performance [Jiang et al., 2021b]. We compare the different UED methods against Domain Randomization (DR) [Tobin et al., 2017], where at each end of an episode, a new network is generated from the parameterized distribution (cf. Section 4.5). We use the implementation provided by the JaxUED library [Coward et al., 2024].

## 5.2 Hyperparameter Tuning

We perform a hyperparameter search using Bayesian-sampling for every discussed algorithm in Section 5.1, with a budget of 250 trials. Each sampled hyperparameter set is trained on 26 host networks, on three separate seeds to evaluate the robustness of the parameters. JAX allows for these three runs to be made in parallel on the same device. We report the aggregated performance of those runs. The performance of a run is reported as the mean solve rate over the set of evaluation levels during the final evaluation phase. After the search, we evaluate the top ten most promising hyperparameters on a set of five seeds, to select the most robust set of parameters. Further details and all the search spaces can be found in Appendix B.

## 6 Experiments

Our experiments investigate three questions: (1) What speed-up does NASimJax achieve compared to the original implementation? (2) Which method for handling large action spaces is better suited to our setting? (3) Which UED methods perform best on zero-shot policy transfer (ZSPT) tasks?

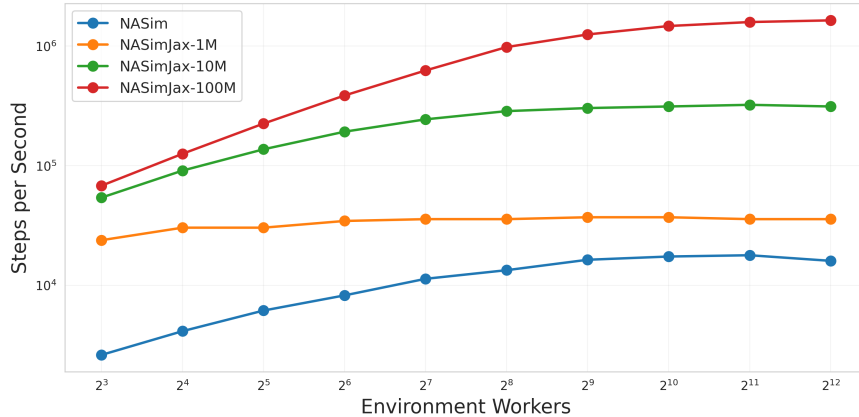


Figure 2: Training speed comparison between NASim with 10M steps of training budget against NASimJax with 1M, 10M and 100M steps. Number of environment workers are doubled every time. Results show the impact of JAX’s JIT-compilation on total runtime. Details of the speed test are available in Section 6.1. The full results are in Appendix A.

## 6.1 Performance Comparison

To investigate the performance increase compared to the original implementation, we perform several training runs with an increasing number of environment workers, starting with 8 and doubling until reaching 4096. We highlight that we train an actual policy, instead of comparing performance of random policies against one another, as this provides a more accurate measure of the performance to be expected when using the environment. For NASim, we use `cleanRL`’s [Huang et al., 2022] implementation of PPO and compare it against NASimJax using the `PureJaxRL`’s [Lu et al., 2022] PPO implementation. We match the hyperparameters, such that we collect the same amount of experience per rollout. The difference in training speeds is shown by Figure 2. At its peak NASimJax trained over 100 million steps achieves a performance of 1.6M steps per second, which amounts to a speed-up of 100 times over the original. The machine we perform these experiments on is equipped with an Intel(R) Xeon(R) Gold 6230R CPU @ 2.10GHz and an NVIDIA RTX A4000. These results pronounce NASimJax’s ability to train policies with a greater budget, as compiling the code takes up a significant amount of time when using small training budgets. We also tried comparing our implementation against CyberBattleSim [Team., 2021], but the environment does not support running parallel environment workers by default, therefore not allowing us to perform the same experiment.

## 6.2 Environment Configurations

Rather than prescribing fixed benchmark scenarios, NASimJax is designed as a configurable research framework. The network generation pipeline exposes a set of parameters: topology density ( $t_d$ ), total host count ( $N_h$ ), service ( $svc_d$ ) and process ( $proc_d$ ) density, sensitive host density ( $s_d$ ) (cf. Section 4.5). These allow researchers to instantiate environments aligned with their specific research interests. To ground the experimental investigation that follows, we describe three reference configurations of increasing complexity that we use throughout this work in Table 1. We emphasize that these are illustrative rather than normative. These scales exceed those typically used in prior simulation-based work—e.g. up to 8 hosts in StochNASim and 16 in PenGym and NASimEmu—though these environments differ in scope and formulation.

A network increases in complexity via two factors: (1) More *active* hosts in the network means a longer horizon, and more unmasked actions. This directly affects the amount of exploration required in the early stages of training before finding good trajectories to bootstrap on. (2) A larger number of hosts, services, processes and OSes directly affects the size of the resulting action space as established in Section 4.2.

Across all configurations, action costs are fixed at 1 for scanning and 3 for exploit and privilege escalation actions. This 3:1 ratio aims to discourage brute-force policies that skip information gathering. The sensitive host reward is  $V_h = 50$  and we provide a host discovery reward of  $V_d = 1$ . These values were chosen to ensure that compromising a sensitive host strongly dominates the action cost signal, while the small discovery

Table 1: Network configuration and topology densities per network size. All configurations use 3 processes, 3 services, 2 operating systems, and  $svc_d = proc_d = 0.7$ . Training densities are **bold**.

Hosts	$N_s$	$s_d$	Steps	$ \mathcal{A} $	Topology Density $t_d$				
16	7	0.20	300	256	<b>0.06</b>	0.115	<b>0.15</b>	0.195	<b>0.24</b>
26	10	0.15	300	416	<b>0.04</b>	0.08	<b>0.12</b>	0.16	<b>0.20</b>
40	16	0.15	500	640	<b>0.03</b>	0.06	<b>0.09</b>	0.12	<b>0.15</b>

reward provides a mild incentive for exploration. Since rewards are scaled by  $N_s \cdot V_h$  during training (cf. Section 5.1.3), the absolute magnitude of  $V_h$  does not affect the normalized learning signal—only the relative ratios between these values matter.

Parameters such as  $t_d$  and  $s_d$  were carefully chosen to enable the generation of networks with a varied number of *active* hosts, as illustrated in Figure 3 (see Appendix C for complete distributions). The  $t_d$  ranges are scaled inversely with network size because larger networks require lower connectivity probabilities to produce meaningful variation in active host counts. At higher densities, most subnets become reachable and the distribution concentrates near the maximum.

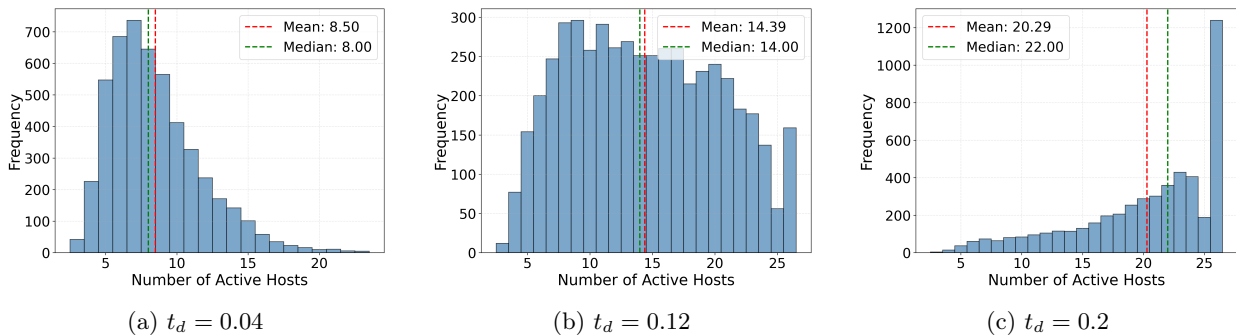


Figure 3: Visualization of  $t_d$ 's effect on active host counts within generated networks of 26 hosts. The full network parameters are displayed in Table 1.

### 6.3 Growing Action Spaces

To compare the performance of our two methods for handling large action spaces, we train both algorithms on the configurations established in Section 6.2 using different training budgets: 100M steps for 16-host networks, 500M for 26 hosts, and 1B for 40 hosts. Each algorithm is trained on five seeds to account for variance. We periodically evaluate the policies in-distribution over 50 networks (using the same  $t_d$ ), as our focus here is on action space scaling rather than out-of-distribution generalization. The results in Figure 4 show that for smaller action spaces (16 hosts), the problem is simple enough that action space decomposition offers no significant benefit. For 26-host networks, however, the advantage of 2SAS's factored action space is clearly pronounced, achieving an 82% solve rate versus flat masking's 66%. This performance gap widens further on 40-host networks, where masking achieves only a 14% solve rate compared to 2SAS's 42%. These results demonstrate that factoring the action space becomes increasingly critical as network scale grows. Hyperparameters for this experiment are provided in Appendix B.2.

### 6.4 Zero-Shot Policy Transfer

The CMDP formulation allows us to vary the training distribution over active hosts via the  $t_d$  parameter. This experiment tests how the choice of training distribution affects generalisation to unseen active host distributions at evaluation time. For every network described in Table 1, we select five topology densities per network size to create varying distributions (cf. Figure 3). The UED algorithms used are DR, PLR,

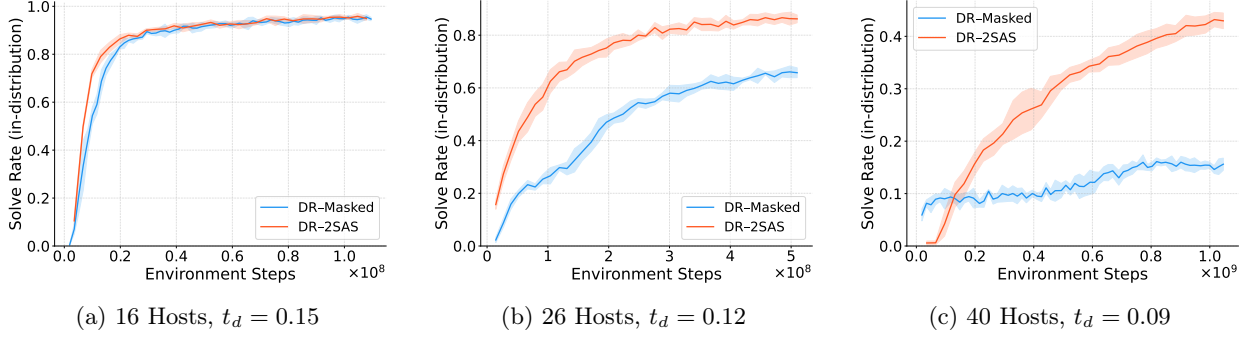


Figure 4: Comparison between standard action masking and 2SAS on 16, 26 and 40 host networks. Both algorithms use DR and evaluate in-distribution performance on 50 evaluation networks. Results are reported over 5 seeds with 95% CI.

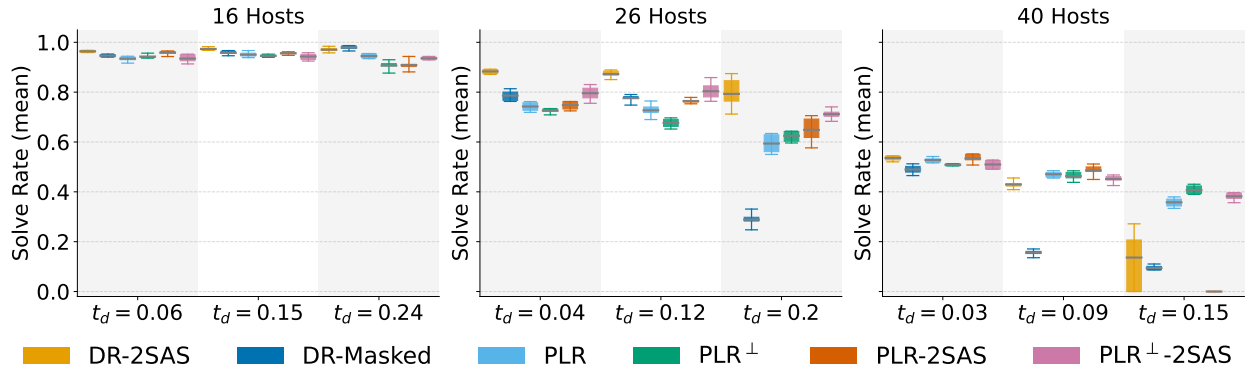


Figure 5: ZSPT across topology densities  $t_d$  for 16-, 26- and 40-host networks. Each algorithm is trained on three values of  $t_d$  (low, mid, high) and evaluated on all other  $t_d$ . Bars show the mean solve rate aggregated over five seeds; boxes span the IQR (Q1–Q3), whiskers the full range.

and  $\text{PLR}^\perp$  (cf. Section 5.1.4), each combined with our two action-space methods—Masking and 2SAS—to further investigate their influence on solve rate on out-of-distribution networks.

For each algorithm, we train three policies, one per density, as highlighted in Table 1. The training budget is the same as in our previous experiment. During training, the policy is periodically evaluated on five sets of 50 evaluation environments, each set using a different  $t_d$ . Hyperparameters for this experiment are provided in Appendix B.2.

The aggregated results are displayed in Figure 5. For 16-host networks, the impact of evaluating on a different  $t_d$  from the one trained on is minor, and all methods achieve comparable mean solve rates close to 0.9. For 26-host networks, differences are more pronounced: training on lower  $t_d$ , which produces fewer active hosts on average, yields the best overall solve rate across all methods. Training at  $t_d = 0.2$  degrades performance for the PLR-based methods, while DR-Masked struggles substantially, averaging only 0.29 across all evaluation densities. DR-2SAS and DR remain comparably strong at low training densities but drop off sharply for denser ones. The two PLR variants exhibit the most consistent performance, leveraging their replay capabilities to construct an implicit curriculum.

For 40-host networks, solve rates are generally lower across all conditions, reflecting the inherent difficulty of this larger task. At  $t_d = 0.09$ , DR-Masked struggles relative to the other methods. The results at  $t_d = 0.15$  are the most striking:  $\text{PLR}^\perp$ -Masked,  $\text{PLR}^\perp$ -2SAS, and  $\text{PLR}^\perp$  all benefit clearly from replay, maintaining strong performance even at this demanding density. DR-2SAS performs close to DR-Masked, but with much higher variance, which we attribute to the host head’s large effective branching factor once the agent has penetrated deeply into the network. Most notably, PLR-2SAS collapses entirely at this density—a failure we analyse in Section 7, where we show it stems from the interaction between PLR’s

episode-reset behaviour, 2SAS’s credit assignment structure, and the resulting failure to populate the replay buffer. We provide complete per-density evaluation curves for all network sizes in Appendix D.

## 7 Discussion

While our experiments focus on ZSPT across network topologies of varying density, the framework is designed to support a broader range of research questions. The number of services and processes can be increased to further exacerbate the large action space problem, and  $t_d$  and  $s_d$  can be tuned to systematically vary task difficulty independently of network size. This positions NASimJax not as a fixed benchmark, but as a configurable platform for investigating the breaking points of current methods under controlled conditions.

**Training context and zero-shot transfer.** The results in Figure 5 reveal that training context matters significantly, and that this effect intensifies with network scale. Training on lower  $t_d$  networks, which produce fewer active hosts on average, consistently yields better generalisation across all tested densities—even those denser than the training distribution. We attribute this to an implicit curriculum effect: sparser topologies expose the agent to shorter-horizon tasks early in training, enabling it to build competence before encountering complex attack paths. This finding has a practical implication: training on computationally cheaper, low-density networks may be preferable to training directly on the target distribution. DR is competitive at lower densities, consistent with findings in other domains [Jiang et al., 2021a, Coward et al., 2024], but degrades substantially when the training distribution is dense. Both PLR variants exploit the curriculum effect more robustly through replay, maintaining stronger performance even when trained at high  $t_d$ .

**Reward scaling.** Beyond training stability, the reward scaling introduced in Section 5.1.3 is a prerequisite for PLR to function correctly in this setting. PLR prioritizes levels based on estimated regret, which is derived from the agent’s returns. Without scaling, regret estimates are biased toward larger networks simply because they accumulate higher raw returns, causing PLR’s level selection to conflate network size with learning potential. Scaling makes regret estimates comparable across contexts, allowing PLR to prioritize levels based on genuine learning progress rather than incidental differences in reward magnitude.

**PLR-2SAS failure at 40 hosts.** A notable result in our 40-host experiments is the complete collapse of PLR-2SAS at  $t_d = 0.15$ , where it fails to achieve any positive solve rate despite PLR-Masked, PLR<sup>+</sup>-2SAS, and PLR<sup>+</sup>-Masked all performing well (Figure 5). We attribute this to three interacting factors. First, PLR’s exploration branch resets all environments to fresh levels at every training step, unlike DR which preserves environment state across rollout windows. At  $t_d = 0.15$ , generated networks contain on average 34 active hosts, making episodes too long to complete within a single rollout. DR-2SAS can work on such levels across consecutive rollouts, accumulating progress; PLR’s exploration branch cannot, producing almost exclusively failed trajectories. Second, these failures are particularly damaging under the two-stage decomposition. Because 2SAS computes a single advantage from the joint (host, action) outcome, it cannot distinguish which stage caused a poor result. A wrong exploit on a correctly chosen host penalises both heads equally, and a wrong host selection penalises the action head for an outcome it had no control over. Without successful episodes to anchor learning, this bidirectional misattribution compounds: a degraded host head presents worse contexts to the action head, producing worse outcomes that further degrade the host head. PLR-Masked avoids this because a flat policy has no decomposed stages between which credit can be misattributed. Third, the near-total absence of successful episodes during exploration means the replay buffer is never adequately populated, so prioritised replay, which could rescue training by curating solvable levels, never activates. PLR<sup>+</sup>-2SAS avoids the failure entirely by withholding gradient updates during exploration, so the two-stage architecture is never damaged by the failed trajectories, and training proceeds exclusively on curated replay levels.

## 8 Conclusion

In this work, we introduced NASimJax, the first pure JAX implementation of an RL environment for penetration testing. By formulating the problem as a partially observable Contextual MDP with a redesigned net-

work generation pipeline producing diverse, realistic, and guaranteed-solvable scenarios, NASimJax provides a principled framework for investigating zero-shot policy transfer to unseen network topologies. Compared to CPU-bound simulators, NASimJax achieves a 100× speed improvement, reaching 1.6M steps per second on a single entry-level GPU. This performance gain unlocks experimentation at scales that were previously infeasible, and the configurable network generation pipeline supports a broad range of research questions beyond those investigated here—from scaling action spaces to studying the effect of network topology on attack complexity.

As an initial demonstration, we leveraged this platform to investigate two open challenges. To address the linearly growing action space, we introduced two-stage action selection (2SAS), which offers no benefit at small scales but substantially outperforms flat masking as networks grow, achieving a 42% versus 14% solve rate on 40-host networks. For zero-shot transfer, we evaluated Domain Randomization and Prioritized Level Replay across topology densities, finding that training on low-density networks consistently yields better generalization than training on the target distribution directly—a practically useful result, as sparse networks are substantially cheaper to train on. Finally, we identify and explain a destructive interaction between PLR’s episode-reset behaviour and 2SAS’s credit assignment structure at larger scales, offering a concrete direction for future work.

## Acknowledgments

This research was funded by the Royal Higher Institute of Defence under the project DAP23/05. Further support comes from the Flemish Government under the “Onderzoeksprogramma Artificiële Intelligentie (AI) Vlaanderen” program. The resources and services used in this work were, in part, provided by the VSC (Flemish Supercomputer Center), funded by the Research Foundation - Flanders (FWO) and the Flemish Government. Pieter Libin acknowledges support from the Research council of the Vrije Universiteit Brussel (OZR-VUB) via grant number OZR3863BOF. We also thank Elli Makdis Antoun, Hicham Azmani, Bram Silue and all other lab members that have provided feedback throughout the creation of this work.

## References

- National Institute of Standards and Technology. Technical guide to information security testing and assessment. Technical Report SP 800-115, NIST, September 2008. URL <https://doi.org/10.6028/NIST.SP.800-115>.
- Jingju Liu, Yue Zhang, Shicheng Zhou, Jiahai Yang, Yuliang Lu, and Xiaofeng Zhong. Autonomous penetration testing using reinforcement learning: A review and perspectives. *Expert Systems with Applications*, page 130219, 2025.
- Volodymyr Mnih, Koray Kavukcuoglu, David Silver, Andrei A Rusu, Joel Veness, Marc G Bellemare, Alex Graves, Martin Riedmiller, Andreas K Fidjeland, Georg Ostrovski, et al. Human-level control through deep reinforcement learning. *Nature*, 518(7540):529–533, 2015.
- OpenAI, Christopher Berner, Greg Brockman, Brooke Chan, Vicki Cheung, Przemysław Dębiak, Christy Dennison, David Farhi, Quirin Fischer, Shariq Hashme, Chris Hesse, Rafal Józefowicz, Scott Gray, Catherine Olsson, Jakub Pachocki, Michael Petrov, Henrique Pondé de Oliveira Pinto, Jonathan Raiman, Tim Salimans, Jeremy Schlatter, Jonas Schneider, Szymon Sidor, Ilya Sutskever, Jie Tang, Filip Wolski, and Susan Zhang. Dota 2 with large scale deep reinforcement learning. 2019a. URL <https://arxiv.org/abs/1912.06680>.
- Oriol Vinyals, Igor Babuschkin, Wojciech M Czarnecki, Michaël Mathieu, Andrew Dudzik, Junyoung Chung, David H Choi, Richard Powell, Timo Ewalds, Petko Georgiev, et al. Grandmaster level in starcraft ii using multi-agent reinforcement learning. *nature*, 575(7782):350–354, 2019.
- Peter R Wurman, Samuel Barrett, Kenta Kawamoto, James MacGlashan, Kaushik Subramanian, Thomas J Walsh, Roberto Capobianco, Alisa Devlic, Franziska Eckert, Florian Fuchs, et al. Outracing champion gran turismo drivers with deep reinforcement learning. *Nature*, 602(7896):223–228, 2022.

- OpenAI, Ilge Akkaya, Marcin Andrychowicz, Maciek Chociej, Mateusz Litwin, Bob McGrew, Arthur Petron, Alex Paino, Matthias Plappert, Glenn Powell, Raphael Ribas, Jonas Schneider, Nikolas Tezak, Jerry Tworek, Peter Welinder, Lilian Weng, Qiming Yuan, Wojciech Zaremba, and Lei Zhang. Solving rubik’s cube with a robot hand. *CoRR*, abs/1910.07113, 2019b. URL <http://arxiv.org/abs/1910.07113>.
- Alexandra Cimpean, Timothy Verstraeten, Lander Willem, Niel Hens, Ann Nowé, and Pieter Libin. Evaluating covid-19 vaccine allocation policies using bayesian  $m$ -top exploration. *arXiv preprint arXiv:2301.12822*, 2023.
- Timothy Verstraeten, Pieter Libin, and Ann Nowé. Fleet control using coregionalized gaussian process policy iteration. In *European Conference on Artificial Intelligence (ECAI 2020)*, pages 1571–1578. IOS Press, 2020.
- Carlos Sarraute, Olivier Buffet, and Jörg Hoffmann. POMDPs Make Better Hackers: Accounting for Uncertainty in Penetration Testing. *Proceedings of the AAAI Conference on Artificial Intelligence*, 26(1): 1816–1824, 2012. ISSN 2374-3468. Number: 1.
- Carlos Sarraute, Olivier Buffet, and Joerg Hoffmann. Penetration Testing == POMDP Solving?, June 2013. arXiv:1306.4714 [cs].
- Gabriel Dulac-Arnold, Nir Levine, Daniel J Mankowitz, Jerry Li, Cosmin Paduraru, Sven Gowal, and Todd Hester. Challenges of real-world reinforcement learning: definitions, benchmarks and analysis. *Machine Learning*, 110(9):2419–2468, 2021.
- Jonathon Schwartz and Hanna Kurniawatti. Nasim: Network attack simulator. <https://networkattacksimulator.readthedocs.io/>, 2019.
- Microsoft Defender Research Team. Cyberbattlesim. <https://github.com/microsoft/cyberbattlesim>, 2021. Created by Christian Seifert, Michael Betser, William Blum, James Bono, Kate Farris, Emily Goren, Justin Grana, Kristian Holsheimer, Brandon Marken, Joshua Neil, Nicole Nichols, Jugal Parikh, Haoran Wei.
- Harry Emerson, Liz Bates, Chris Hicks, and Vasilios Mavroudis. Cyborg++: An enhanced gym for the development of autonomous cyber agents. *arXiv preprint arXiv:2410.16324*, 2024.
- Andrew Patterson, Samuel Neumann, Martha White, and Adam White. Empirical design in reinforcement learning. *Journal of Machine Learning Research*, 25(318):1–63, 2024.
- Jacob Adkins, Michael Bowling, and Adam White. A method for evaluating hyperparameter sensitivity in reinforcement learning. *Advances in Neural Information Processing Systems*, 37:124820–124842, 2024.
- Dibya Ghosh, Jad Rahme, Aviral Kumar, Amy Zhang, Ryan P Adams, and Sergey Levine. Why generalization in rl is difficult: Epistemic pomdps and implicit partial observability. *Advances in neural information processing systems*, 34:25502–25515, 2021.
- Robert Kirk, Amy Zhang, Edward Grefenstette, and Tim Rocktäschel. A Survey of Zero-shot Generalisation in Deep Reinforcement Learning. *jair*, 76:201–264, January 2023. ISSN 1076-9757. doi: 10.1613/jair.1.14174. URL <http://jair.org/index.php/jair/article/view/14174>.
- Josh Tobin, Rachel Fong, Alex Ray, Jonas Schneider, Wojciech Zaremba, and Pieter Abbeel. Domain randomization for transferring deep neural networks from simulation to the real world. In *2017 IEEE/RSJ International Conference on Intelligent Robots and Systems (IROS)*, pages 23–30, 2017. doi: 10.1109/IROS.2017.8202133.
- Minqi Jiang, Edward Grefenstette, and Tim Rocktäschel. Prioritized level replay. In *International Conference on Machine Learning*, pages 4940–4950. PMLR, 2021a.
- Martin L. Puterman. Chapter 8 markov decision processes. In *Stochastic Models*, volume 2 of *Handbooks in Operations Research and Management Science*, pages 331–434. Elsevier, 1990.

- Richard S. Sutton and Andrew G. Barto. *Reinforcement Learning: An Introduction*. A Bradford Book, Cambridge, MA, USA, 2018. ISBN 0262039249.
- Assaf Hallak, Dotan Di Castro, and Shie Mannor. Contextual markov decision processes. *arXiv preprint arXiv:1502.02259*, 2015.
- James Bradbury, Roy Frostig, Peter Hawkins, Matthew James Johnson, Chris Leary, Dougal Maclaurin, George Necula, Adam Paszke, Jake VanderPlas, Skye Wanderman-Milne, and Qiao Zhang. JAX: composable transformations of Python+NumPy programs, 2018. URL <http://github.com/jax-ml/jax>.
- Alexander Rutherford, Benjamin Ellis, Matteo Gallici, Jonathan Cook, Andrei Lupu, Garð ar Ingvarsson, Timon Willi, Ravi Hammond, Akbir Khan, Christian Schroeder de Witt, Alexandra Souly, Saptarashmi Bandyopadhyay, Mikayel Samvelyan, Minqi Jiang, Robert Lange, Shimon Whiteson, Bruno Lacerda, Nick Hawes, Tim Rocktäschel, Chris Lu, and Jakob Foerster. Jaxmarl: Multi-agent rl environments and algorithms in jax. In A. Globerson, L. Mackey, D. Belgrave, A. Fan, U. Paquet, J. Tomczak, and C. Zhang, editors, *Advances in Neural Information Processing Systems*, volume 37, pages 50925–50951. Curran Associates, Inc., 2024. doi: 10.52202/079017-1612. URL [https://proceedings.neurips.cc/paper\\_files/paper/2024/file/5aae125f052c90e326dcf6f380df94f6-Paper-Datasets\\_and\\_Benchmarks\\_Track.pdf](https://proceedings.neurips.cc/paper_files/paper/2024/file/5aae125f052c90e326dcf6f380df94f6-Paper-Datasets_and_Benchmarks_Track.pdf).
- Robert Tjarko Lange. gymmax: A JAX-based reinforcement learning environment library, 2022. URL <http://github.com/RobertTLange/gymmax>.
- Michael Matthews, Michael Beukman, Benjamin Ellis, Mikayel Samvelyan, Matthew Jackson, Samuel Coward, and Jakob Foerster. Craftax: A lightning-fast benchmark for open-ended reinforcement learning. In *International Conference on Machine Learning (ICML)*, 2024.
- Clément Bonnet, Daniel Luo, Donal Byrne, Shikha Surana, Sasha Abramowitz, Paul Duckworth, Vincent Coyette, Laurence I. Midgley, Elshadai Tegegn, Tristan Kalloniatis, Omayma Mahjoub, Matthew Macfarlane, Andries P. Smit, Nathan Grinsztajn, Raphael Boige, Cemlyn N. Waters, Mohamed A. Mimouni, Ulrich A. Mbou Sob, Ruan de Kock, Siddarth Singh, Daniel Furelos-Blanco, Victor Le, Arnú Pretorius, and Alexandre Laterre. Jumanji: a diverse suite of scalable reinforcement learning environments in jax, 2024. URL <https://arxiv.org/abs/2306.09884>.
- Jaromír Janisch, Tomáš Pevný, and Viliam Lisý. NASimEmu: Network Attack Simulator & Emulator for Training Agents Generalizing to Novel Scenarios, August 2023. arXiv:2305.17246 [cs].
- Huynh Phuong Thanh Nguyen, Kento Hasegawa, Kazuhide Fukushima, and Razvan Beuran. Pengym: Realistic training environment for reinforcement learning pentesting agents. *Computers & Security*, 148: 104140, 2025. ISSN 0167-4048. doi: <https://doi.org/10.1016/j.cose.2024.104140>. URL <https://www.sciencedirect.com/science/article/pii/S0167404824004450>.
- Raphael Simon, Pieter Libin, and Wim Mees. Learning robust penetration-testing policies under partial observability: A systematic evaluation, 2025. URL <https://arxiv.org/abs/2509.20008>.
- Franco Terranova, Abdelkader Lahmadi, and Isabelle Chrisment. Scalable and generalizable rl agents for attack path discovery via continuous invariant spaces. In *2025 28th International Symposium on Research in Attacks, Intrusions and Defenses (RAID)*, page 18, 2025.
- Karl Cobbe, Oleg Klimov, Chris Hesse, Taehoon Kim, and John Schulman. Quantifying generalization in reinforcement learning. In *International conference on machine learning*, pages 1282–1289. PMLR, 2019.
- Chris Lu, Jakub Kuba, Alistair Letcher, Luke Metz, Christian Schroeder de Witt, and Jakob Foerster. Discovered policy optimisation. *Advances in Neural Information Processing Systems*, 35:16455–16468, 2022.
- Zegang Li, Qian Zhang, and Guangwen Yang. EPPTA: Efficient partially observable reinforcement learning agent for penetration testing applications. n/a:e12818, 2023. ISSN 2577-8196. \_eprint: <https://onlinelibrary.wiley.com/doi/pdf/10.1002/eng2.12818>.

- Franco Terranova, Abdelkader Lahmadi, and Isabelle Chrisment. Leveraging deep reinforcement learning for cyber-attack paths prediction: Formulation, generalization, and evaluation. In *Proceedings of the 27th International Symposium on Research in Attacks, Intrusions and Defenses*, pages 1–16, 2024.
- Anssi Kanervisto, Christian Scheller, and Ville Hautamäki. Action space shaping in deep reinforcement learning. In *2020 IEEE conference on games (CoG)*, pages 479–486. IEEE, 2020.
- Shengyi Huang and Santiago Ontañón. A Closer Look at Invalid Action Masking in Policy Gradient Algorithms. *The International FLAIRS Conference Proceedings*, 35, May 2022. ISSN 2334-0762. arXiv:2006.14171 [cs, stat].
- Julien Perolat, Bart De Vylder, Daniel Hennes, Eugene Tarassov, Florian Strub, Vincent de Boer, Paul Muller, Jerome T Connor, Neil Burch, Thomas Anthony, et al. Mastering the game of stratego with model-free multiagent reinforcement learning. *Science*, 378(6623):990–996, 2022.
- Hado P Van Hasselt, Arthur Guez, Matteo Hessel, Volodymyr Mnih, and David Silver. Learning values across many orders of magnitude. *Advances in neural information processing systems*, 29, 2016.
- Karl Cobbe, Christopher Hesse, Jacob Hilton, and John Schulman. Leveraging procedural generation to benchmark reinforcement learning. In *Proceedings of the 37th International Conference on Machine Learning*, ICML’20. JMLR.org, 2020.
- Minqi Jiang, Michael Dennis, Jack Parker-Holder, Jakob Foerster, Edward Grefenstette, and Tim Rocktäschel. Replay-guided adversarial environment design. In M. Ranzato, A. Beygelzimer, Y. Dauphin, P.S. Liang, and J. Wortman Vaughan, editors, *Advances in Neural Information Processing Systems*, volume 34, pages 1884–1897. Curran Associates, Inc., 2021b. URL [https://proceedings.neurips.cc/paper\\_files/paper/2021/file/0e915db6326b6fb6a3c56546980a8c93-Paper.pdf](https://proceedings.neurips.cc/paper_files/paper/2021/file/0e915db6326b6fb6a3c56546980a8c93-Paper.pdf).
- Samuel Coward, Michael Beukman, and Jakob Foerster. Jaxued: A simple and useable ued library in jax. *arXiv preprint*, 2024.
- Shengyi Huang, Rousslan Fernand Julien Dossa, Chang Ye, Jeff Braga, Dipam Chakraborty, Kinal Mehta, and João G.M. Araújo. Cleanrl: High-quality single-file implementations of deep reinforcement learning algorithms. *Journal of Machine Learning Research*, 23(274):1–18, 2022.

## A Speed Comparison Details

Table 2 showcases the full details of our experiment in Section 6.1.

Table 2: Performance Comparison of NASim and NASimJax Implementations

Num Envs	NASim		NASimJax-1M		NASimJax-10M		NASimJax-100M	
	Time (s)	Steps/s	Time (s)	Steps/s	Time (s)	Steps/s	Time (s)	Steps/s
8	3823	2,616	42	23,810	185	54,054	1471	67,981
16	2420	4,132	33	30,303	110	90,909	796	125,628
32	1627	6,146	33	30,303	73	136,986	445	224,719
64	1215	8,230	29	34,483	52	192,308	259	386,100
128	883	11,325	28	35,714	41	243,902	160	625,000
256	748	13,369	28	35,714	35	285,714	102	980,392
512	612	16,340	27	37,037	33	303,030	80	1,250,000
1024	575	17,391	27	37,037	32	312,500	68	1,470,588
2048	561	17,825	28	35,714	31	322,581	63	1,587,302
4096	625	16,000	28	35,714	32	312,500	61	1,639,344

## B Hyperparameters

This section discusses the search ranges and the exact hyperparameters we’ve selected for the experiments in Section 6. Some more information regarding the tuning strategy: We first tuned both DR methods, and then based on these results, limited the search space for the PLR-based methods. The ranges selected for the PLR-based methods are based on the original works of Jiang et al. [Jiang et al., 2021a,b].

### B.1 Hyperparameter Ranges

Table 3: Hyperparameter Search Ranges: Masked PPO with DR

Hyperparameter	Considered Values
Learning Rate (LR)	{3e-5, 5e-5, 1e-4, 3e-4, 5e-4}
# Environments	{1024}
# Steps	{16, 32, 64, 128}
Layer Size	{256, 512}
Activation Function	{tanh}
Discount Factor ( $\gamma$ )	{0.975, 0.99, 0.995}
GAE Lambda ( $\lambda$ )	{0.8, 0.9, 0.95}
Clip Epsilon	{0.1, 0.2, 0.3}
Entropy Coef.	{0.005, 0.01, 0.02, 0.05}
Max Gradient Norm	{0.5, 1.0, 1.5}
Value Function Coef.	{0.25, 0.5, 1.0}
Update Epochs	{4}

### B.2 Experiment Hyperparameters

The following hyperparameters were held constant across all algorithms and network sizes: number of environments (1024), activation function (**tanh**), discount factor (0.995), and number of update epochs (4). For PLR and PLR<sup>+</sup> variants, the level buffer capacity (10,000), minimum fill ratio (0.5), prioritization strategy (rank-based), and top-*k* (disabled) were additionally held constant.

Table 4: Hyperparameter Search Ranges: PPO-2SAS with DR

Hyperparameter	Considered Values
Learning Rate (LR)	{5e-5, 1e-4, 2e-4, 3e-4, 5e-4}
# Environments	{1024}
# Steps	{16, 32, 64, 128}
Layer Size	{256, 512}
Activation Function	{tanh}
Discount Factor ( $\gamma$ )	{0.975, 0.99, 0.995}
GAE Lambda ( $\lambda$ )	{0.8, 0.9, 0.95}
Clip Epsilon	{0.1, 0.2, 0.3}
Host Entropy Coef.	{0.01, 0.02, 0.05, 0.08}
Action Entropy Coef.	{0.005, 0.01, 0.02, 0.05}
Host Embedding Dim	{16, 32, 64}
Max Gradient Norm	{0.5, 1.0, 1.5}
Value Function Coef.	{0.25, 0.5, 1.0}
Update Epochs	{4}

Table 5: Hyperparameter Search Ranges: PLR and PLR<sup>⊥</sup>

Hyperparameter	Considered Values
Learning Rate (LR)	{2e-4, 3e-4, 5e-4}
# Steps	{32, 64, 128}
GAE Lambda ( $\lambda$ )	{0.8, 0.95}
Clip Epsilon	{0.1, 0.2, 0.3}
Entropy Coef.	{0.005, 0.01, 0.05}
Replay Probability ( $\rho$ )	{0.5, 0.7, 0.9}
Staleness Coefficient ( $\omega$ )	{0.1, 0.3, 0.5, 0.7}
Temperature ( $\beta$ )	{0.1, 0.5, 1.0, 1.4, 2.0}
Level Buffer Capacity	{5000, 10000}
Score Function	{MaxMC, PVL}
Prioritization	{Rank, Top- $k$ }
Top- $k$ ( $k$ )	{5, 25, 50, 100}

Table 6: Hyperparameters for DR (Masked and 2SAS variants) across 16, 26, and 40 host networks.

Hyperparameter	DR (Masked)			DR (2SAS)		
	16h	26h	40h	16h	26h	40h
Learning Rate	3e-4	3e-4	3e-4	2e-4	1e-4	1e-4
# Steps	32	128	64	64	128	128
Layer Size	512	512	512	256	512	512
GAE Lambda ( $\lambda$ )	0.8	0.8	0.8	0.8	0.9	0.8
Clip Epsilon	0.1	0.2	0.1	0.1	0.2	0.1
Entropy Coef.	0.005	0.005	0.005	-	-	-
Host Ent. Coef.	-	-	-	0.01	0.01	0.02
Action Ent. Coef.	-	-	-	0.01	0.01	0.02
Host Embedding Dim	-	-	-	64	64	32
Max Grad Norm	1.0	0.5	0.5	0.5	0.5	0.5
Value Coef.	1.0	0.5	0.25	0.25	1.0	0.5

## C Active Host Distributions

Here we present the full set of distributions for the  $t_d$ -values established in Table 1. As we've selected to use five values for each number of total hosts in the network, we present the resulting distributions in Figures 6, 7 and 8. These clearly showcase the shift in active hosts given  $t_d$ .

## D Extended Results

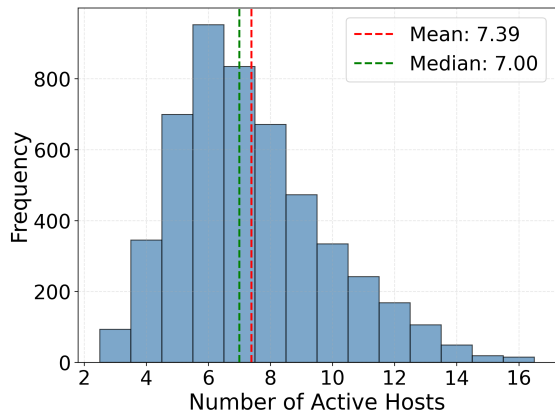
In this Section we highlight some extended results for the experiments conducted in Section 6.4, which showcases the aggregated evaluation performance given different training  $t_d$ -values. Figures 9, 10 11 display more detailed results, where we plot for every algorithm and  $t_d$ -train value the performance against the evaluation  $t_d$ -values.

Table 7: Hyperparameters for PLR (Masked and 2SAS variants) across 16, 26, and 40 host networks.

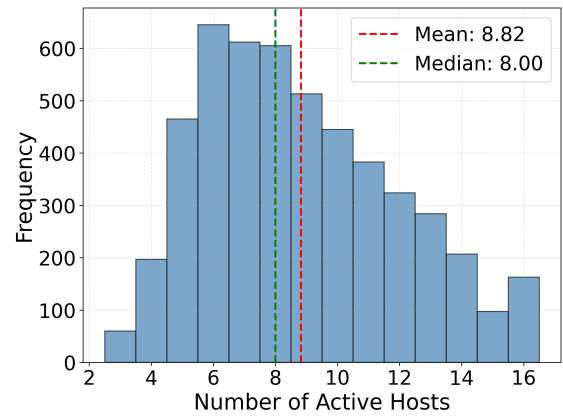
Hyperparameter	PLR (Masked)			PLR (2SAS)		
	16h	26h	40h	16h	26h	40h
Learning Rate	3e-4	3e-4	3e-4	2e-4	1e-4	1e-4
# Steps	128	64	64	128	128	128
Layer Size	512	512	512	512	512	512
GAE Lambda ( $\lambda$ )	0.8	0.8	0.8	0.9	0.95	0.8
Clip Epsilon	0.3	0.3	0.3	0.2	0.2	0.1
Entropy Coef.	0.01	0.005	0.01	–	–	–
Host Ent. Coef.	–	–	–	0.005	0.01	0.02
Action Ent. Coef.	–	–	–	0.01	0.01	0.02
Host Embedding Dim	–	–	–	32	16	32
Max Grad Norm	0.5	0.5	0.5	1.0	1.5	0.5
Value Coef.	0.5	0.5	0.5	1.0	0.25	0.5
Replay Prob. ( $\rho$ )	0.5	0.5	0.5	0.5	0.5	0.9
Staleness ( $\omega$ )	0.7	0.3	0.5	0.3	0.1	0.5
Temperature ( $\beta$ )	0.1	2.0	2.0	2.0	2.0	2.0
Score Function	PVL	MaxMC	MaxMC	MaxMC	PVL	MaxMC

Table 8: Hyperparameters for PLR<sup>⊥</sup> (Masked and 2SAS variants) across 16, 26, and 40 host networks.

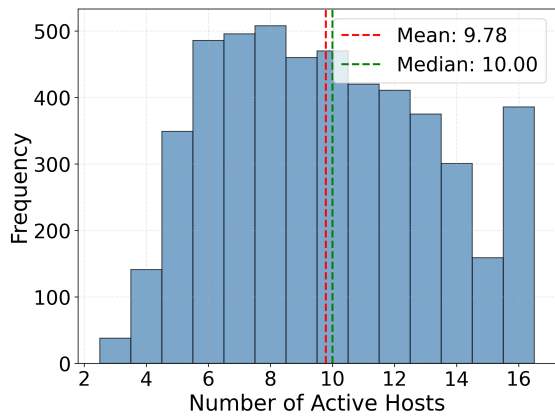
Hyperparameter	PLR <sup>⊥</sup> (Masked)			PLR <sup>⊥</sup> (2SAS)		
	16h	26h	40h	16h	26h	40h
Learning Rate	3e-4	3e-4	3e-4	2e-4	2e-4	1e-4
# Steps	128	128	128	128	128	128
Layer Size	512	512	512	512	512	512
GAE Lambda ( $\lambda$ )	0.95	0.95	0.95	0.95	0.95	0.8
Clip Epsilon	0.3	0.3	0.3	0.3	0.3	0.1
Entropy Coef.	0.005	0.005	0.005	–	–	–
Host Ent. Coef.	–	–	–	0.005	0.01	0.02
Action Ent. Coef.	–	–	–	0.01	0.005	0.02
Host Embedding Dim	–	–	–	32	16	32
Max Grad Norm	0.5	0.5	0.5	1.5	0.5	0.5
Value Coef.	0.5	0.5	0.5	1.0	0.25	0.5
Replay Prob. ( $\rho$ )	0.9	0.9	0.9	0.9	0.9	0.9
Staleness ( $\omega$ )	0.1	0.5	0.1	0.7	0.3	0.5
Temperature ( $\beta$ )	2.0	2.0	2.0	2.0	2.0	2.0
Score Function	MaxMC	MaxMC	MaxMC	MaxMC	MaxMC	MaxMC



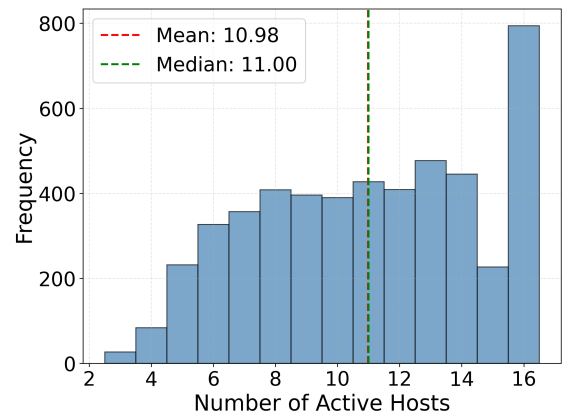
(a)



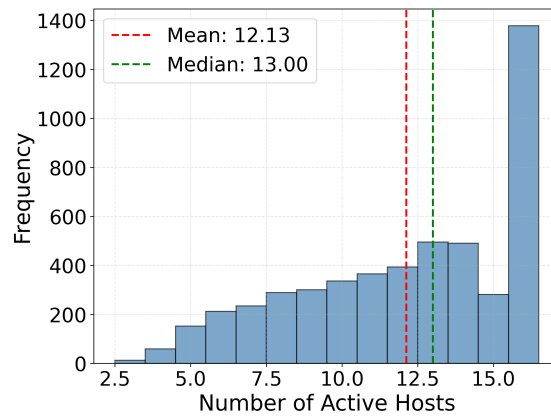
(b)



(c)

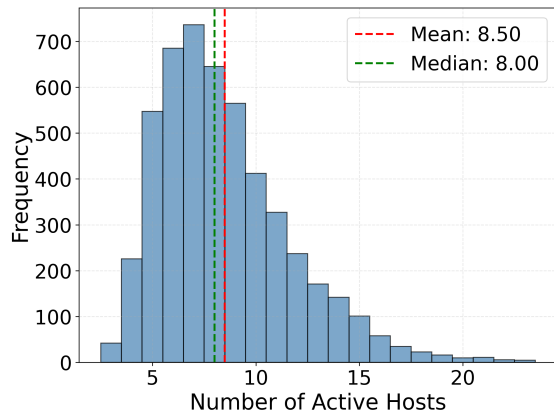


(d)

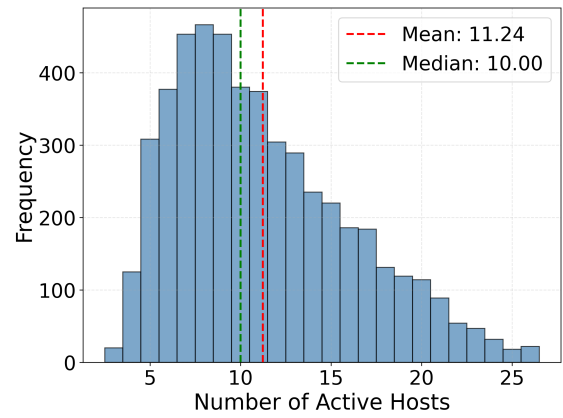


(e)

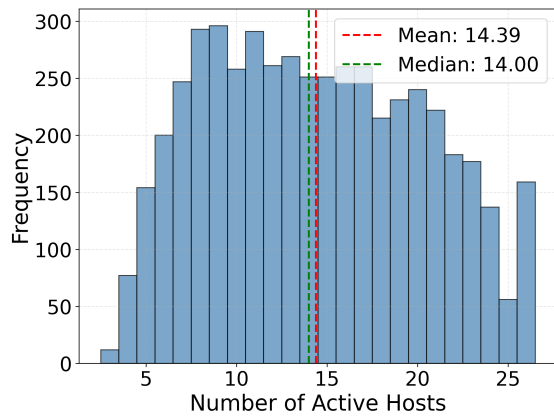
Figure 6: Distributions of active hosts within 16 host networks and how the topology density ( $t_d$ ) parameter influences them.



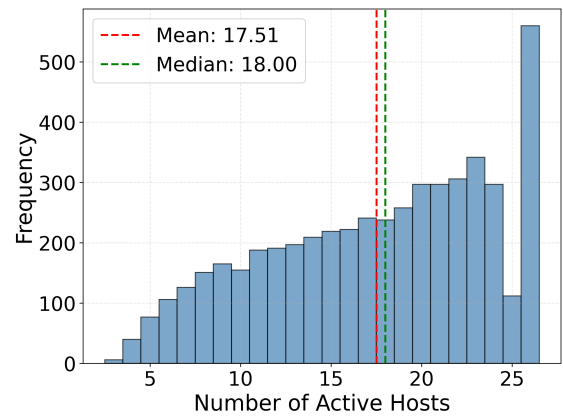
(a)  $t_d = 0.04$



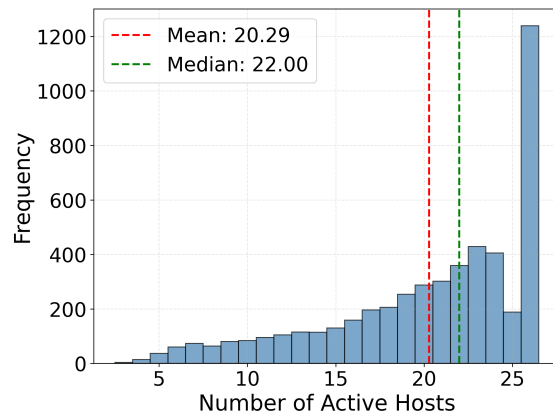
(b)  $t_d = 0.08$



(c)  $t_d = 0.12$

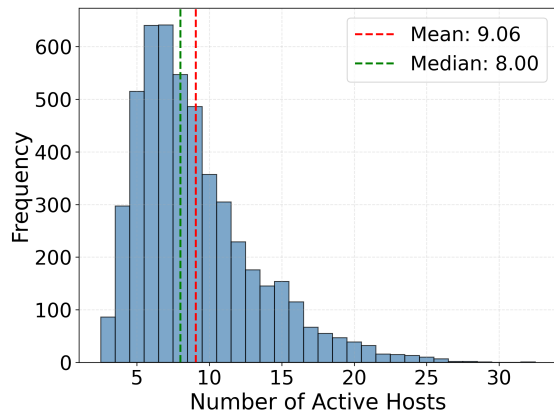


(d)  $t_d = 0.16$

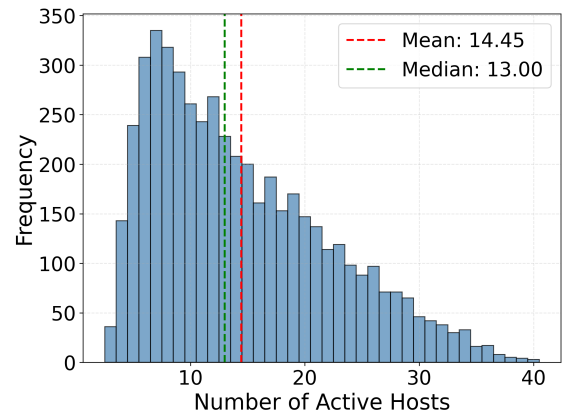


(e)  $t_d = 0.2$

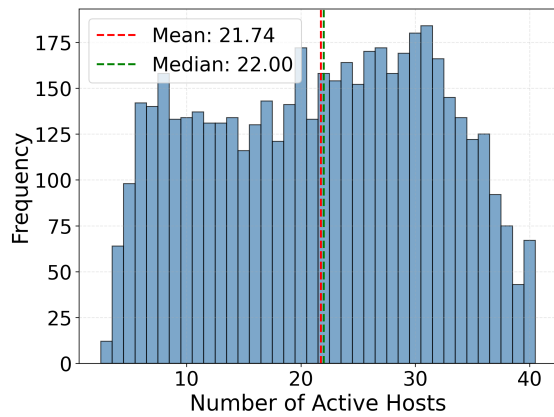
Figure 7: Distributions of active hosts within 26 host networks and how the topology density ( $t_d$ ) parameter influences them.



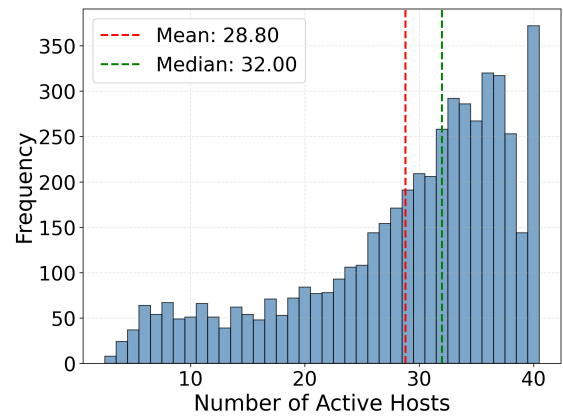
(a)



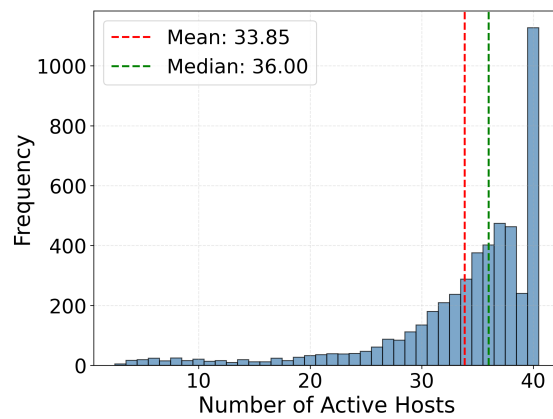
(b)



(c)



(d)



(e)

Figure 8: Distributions of active hosts for 40 host networks and how the topology density ( $t_d$ ) parameter influences them.

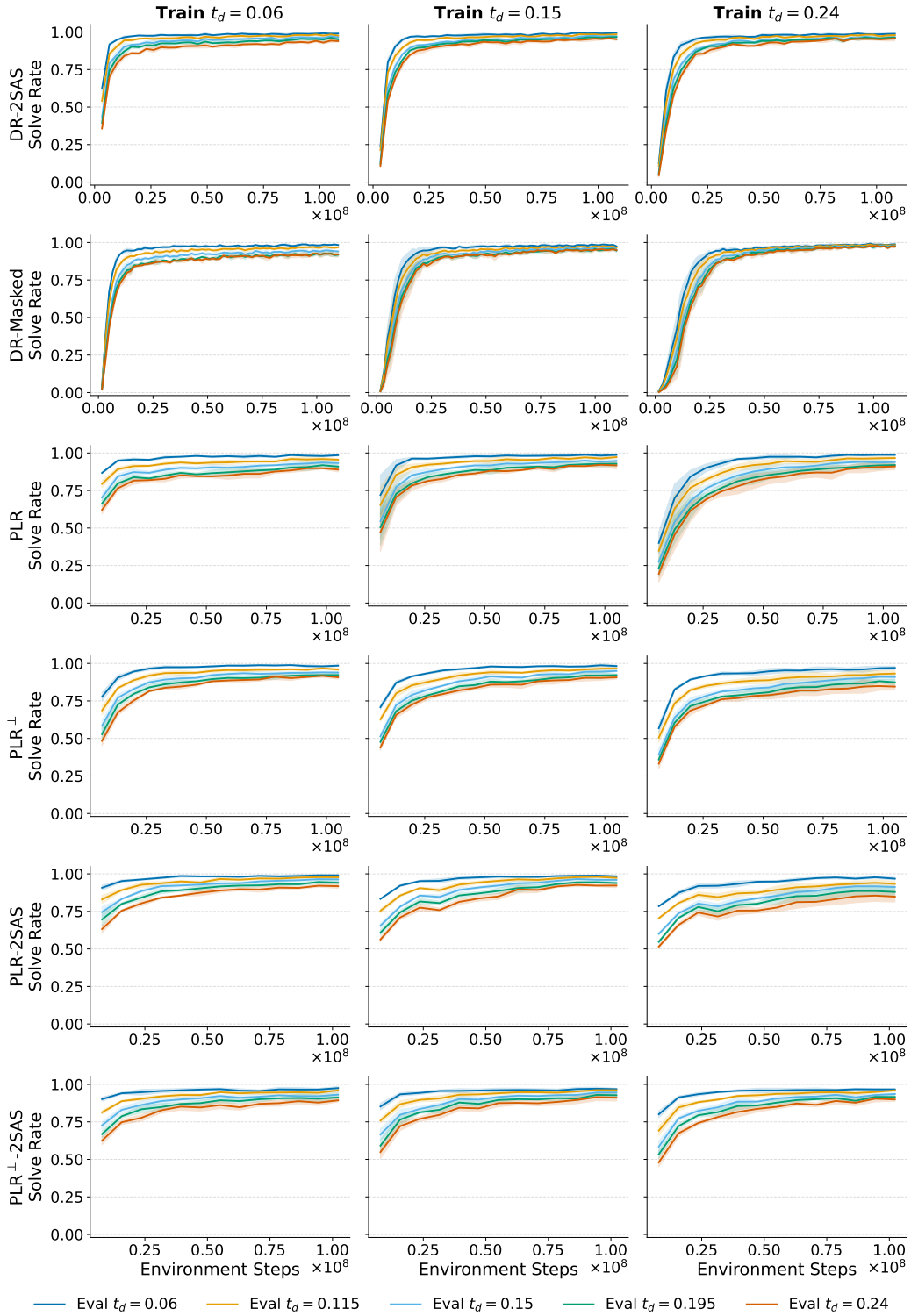


Figure 9: Evaluation curves for 16 host networks. Every column represents the network’s  $t_d$  the policy was trained on. The plots show the evaluation performance against all other selected  $t_d$  for the given network size, as displayed in Table 1.

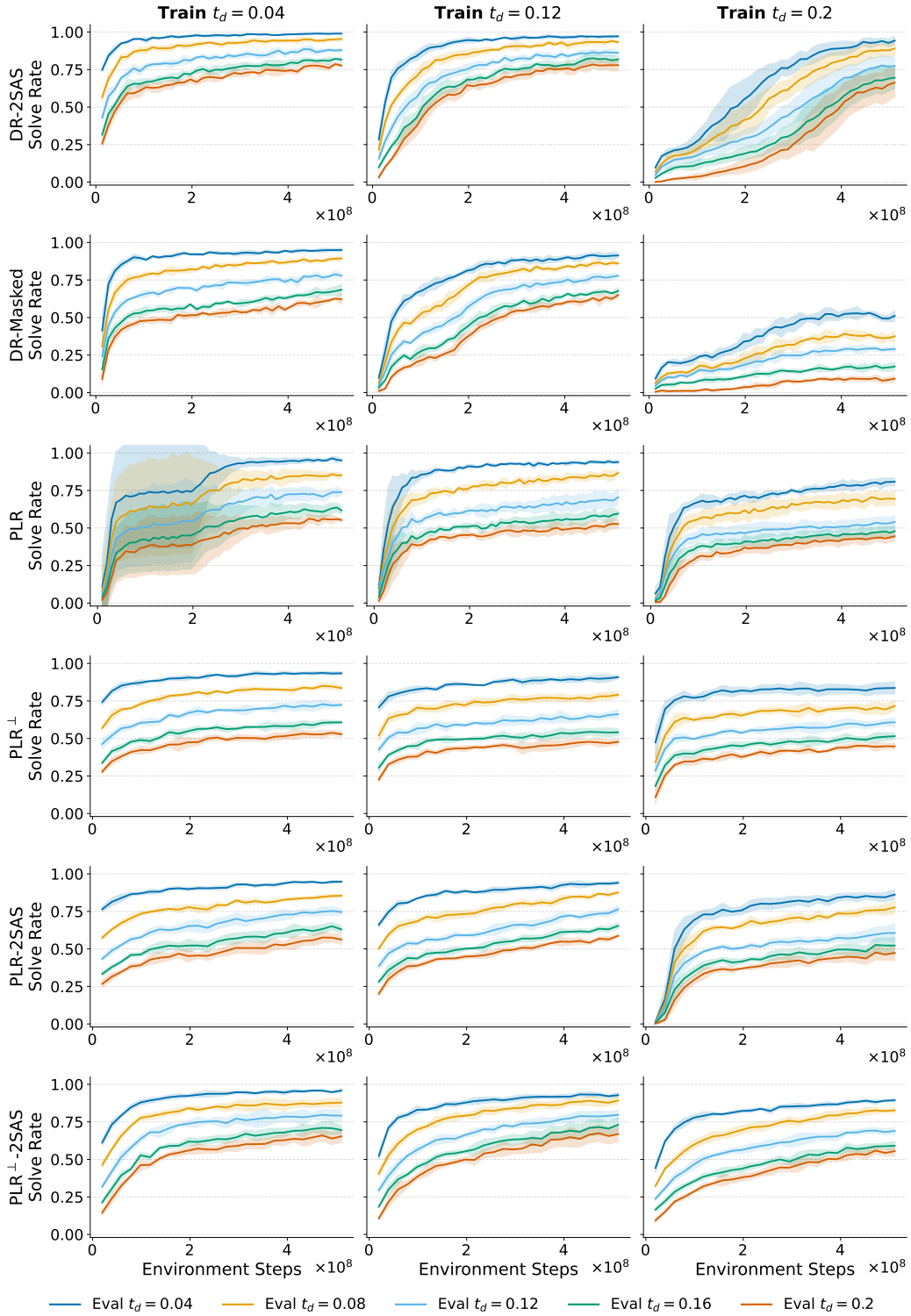


Figure 10: Evaluation curves for 26 host networks. Every column represents the network’s  $t_d$  the policy was trained on. The plots show the evaluation performance against all other selected  $t_d$  for the given network size, as displayed in Table 1.

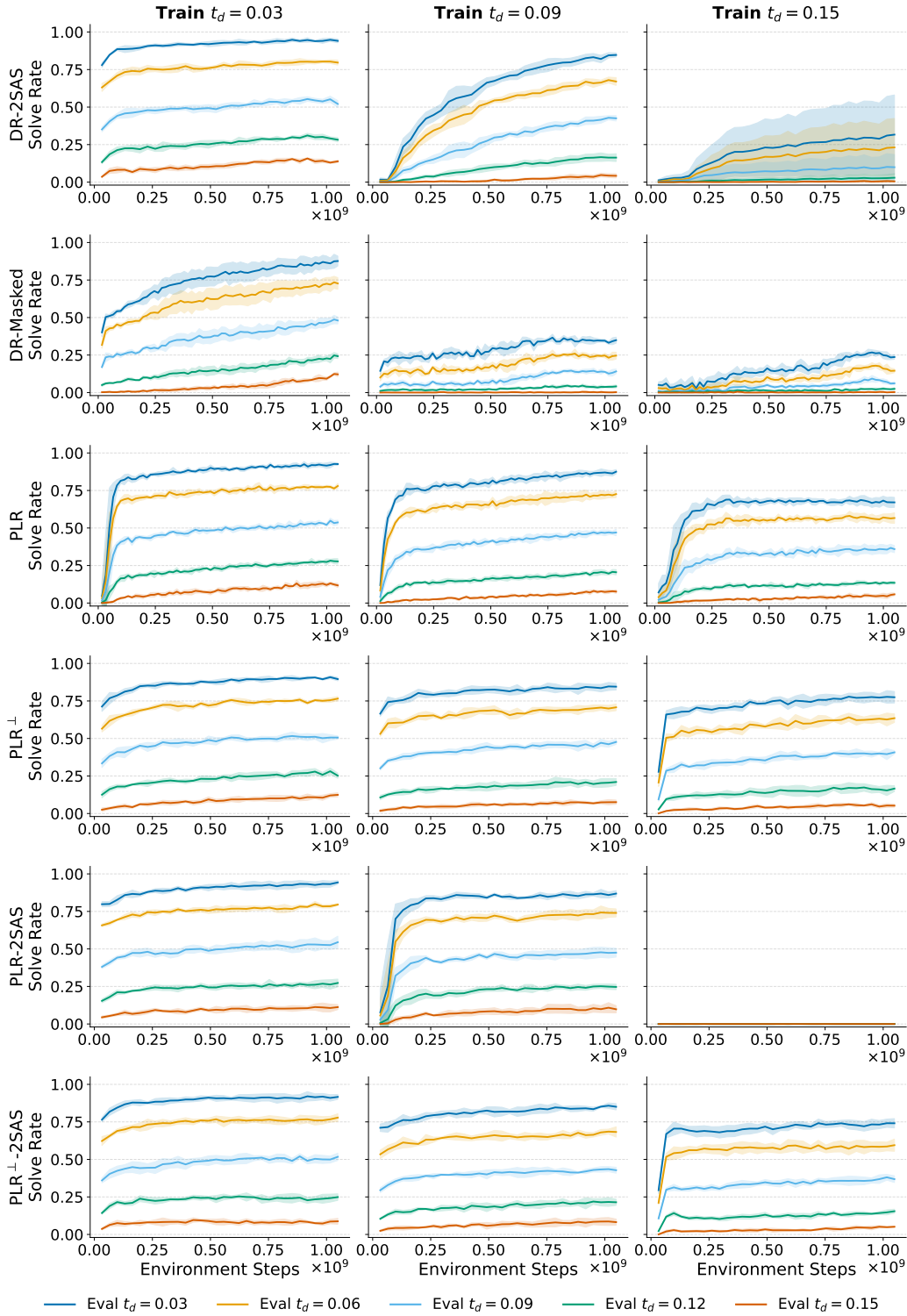


Figure 11: Evaluation curves for 40 host networks. Every column represents the network's  $t_d$  the policy was trained on. The plots show the evaluation performance against all other selected  $t_d$  for the given network size, as displayed in Table 1.